Postprint

This is the accepted version of a paper published in *Advanced Materials Interfaces*. This paper has been peer-reviewed but does not include the final publisher proof-corrections or journal pagination.

Access to the published version may require subscription.

N.B. When citing this work, cite the original published paper.

Permanent link to this version:
http://urn.kb.se/resolve?urn=urn:nbn:se:uu:diva-343670

Passivation of interfaces in thin film solar cells: understanding the effects of a nanostructured rear point contact layer

P. M. P. Salomé[1,2*], Bart Vermang[3,4,5], R. Ribeiro-Andrade [1,6], J. P. Teixeira[2], J. M. V. Cunha[1,7], M. J. Mendes[7], S. Haque[7], J. Borme[1], H. Aguas[7], E. Fortunato[7], R. Martins[7], J. C. González[6], J. P. Leitão[2], P. A. Fernandes[1,2,8], M. Edoff[9] and S. Sadewasser[1]

(1) International Iberian Nanotechnology Laboratory, 4715-330 Braga, Portugal

(2) Departamento de Física and I3N, Universidade de Aveiro, 3810-193 Aveiro, Portugal

(3) University of Hasselt – partner in Solliance, Agoralaan gebouw H, Diepenbeek, 3590, Belgium

(4) Imec – partner in Solliance, Kapeldreef 75, Leuven, 3001, Belgium

(5) Imomec – partner in Solliance, Wetenschapspark 1, Diepenbeek, 3590, Belgium

(6) Departamento de Física, Universidade Federal de Minas Gerais, 30123-970 Belo Horizonte, Minas Gerais, Brazil

(7) i3N/CENIMAT, Department of Materials Science, Faculty of Science and Technology, Universidade NOVA de Lisboa and CEMOP/UNINOVA, Campus de Caparica, 2829-516 Caparica, Portugal

(8) CIETI, Departamento de Física, Instituto Superior de Engenharia do Porto, Instituto Politécnico do Porto, Rua Dr. António Bernardino de Almeida, 431, 4200-072 Porto, Portugal

(9) Ångström Laboratory, Solid State Electronics, Ångström Solar Center, Uppsala University, SE-751 21 Uppsala, Sweden

*corresponding author: P.M.P. Salomé - pedro.salome@inl.int

Keywords: Cu(In,Ga)Se$_2$ (CIGS), thin film solar cells, passivation, photovoltaics, nanofabrication, semiconductors

1

Abstract Thin film solar cells based in Cu(In,Ga)Se$_2$ (CIGS) are among the most efficient polycrystalline solar cells, surpassing CdTe and even polycrystalline silicon solar cells. For further developments, the CIGS technology has to start incorporating different solar cell architectures and strategies that allow for very low interface recombination. In this work, we study and characterize ultrathin 350 nm CIGS solar cells with a rear interface passivation strategy. The rear passivation was achieved using an Al$_2$O$_3$ nanopatterned point structure. Using the cell results, photoluminescence measurements and detailed optical simulations based on the experimental results, we show that by including the nanopatterned point contact structure, the interface defect concentration lowers, which ultimately leads to an increase of solar cell electrical performance mostly by increase of the open circuit voltage. Gains to the short circuit current are distributed between an increased rear optical reflection and also due to electrical effects. Our approach of mixing several techniques allowed us to make a discussion considering the different passivation gains which has not been done in detail in previous works. A solar cell with a nanopatterned rear contact and a 350 nm thick CIGS absorber provided an average power conversion efficiency close to 10%.

Introduction

Cu(In,Ga)Se$_2$ (CIGS) thin film solar cells are currently the highest performing multi-crystalline solar cells available [1] with the record cell achieving a power conversion efficiency value of 22.8% [2]. Large progress has been made in recent years with the introduction of an alkali post-deposition treatment (PDT) that improves the CIGS front interface electrical properties [3,4]. The improvement is a continuation of the CIGS community efforts to increase the quality of the polycrystalline CIGS semiconductor. Likewise, in order to achieve its maximum theoretical efficiency of approximately 33% and to be mass-deployed, other improvements have to be developed [5,6]. Whereas PDT is used to reduce the front interface recombination, the rear interface of the most efficient solar cells combines an interface which also requires improvements. Hence, the study of interface passivation is of the

2

utmost importance if we want to design new CIGS device architectures that permit achieving even higher levels of electrical performance. Furthermore, the study of interface defects and its recombination velocity is important for all types of solar cells like dye-sensitized solar cells [7,8], CdTe [9,10] and perovskite solar cells [11–14], as an example.

It has been demonstrated that the rear interface can be effectively passivated by an Al_2O_3 nanopatterned layer forming a point contact structure [15–18]. Such passivation layer can lead to three advantageous effects: i) chemical passivation; ii) field effect passivation; iii) increased reflection at the rear contact; all while maintaining good electrical contact and devices with high fill factors. Chemical passivation, a terminology coming from the silicon technology, is simply related with a reduction on the interface defect density and it is still an electronic effect. Semiconductor surfaces, especially semiconductor-metal interfaces, can host several interface defects, leading to high surface recombination velocities, which in turn lower the electrical performance of solar cells. Simply, the chemical passivation allows for the decrease of the total number of electrically active defects. The field effect passivation occurs by the presence of a built-in electric field that arises from the high density of fixed charge from the commonly used dielectric materials of the passivation layer. Such field is beneficial for the electrical performance of the solar cell since it drives minority carriers away from the highly recombinative rear contact into the space charge region. While the Al_2O_3 layer is an insulator and acts as a passivation material, the rear electrical contact is established by opening an array of holes in the Al_2O_3 layer. These openings, also called point contacts, are needed to allow electrical contact between the rear electrode, Mo, and the absorber layer, CIGS, while maintaining most of the surface passivated. Furthermore, in order to have a small contact area value, above 95%, and due to the low CIGS carriers´ short diffusion length and lifetime, the dimensions of the openings together with the distance among them need to be close or on the sub-micrometer range [19,20]. Moreover, according to the dimensions of the passivation layer and the refractive index of its material, this layer can also increase the light reflection of the rear contact, allowing for more light to be absorbed by the CIGS layer. While several studies have already shown proof-of-concepts of the point

contact structure [21–24] and of the passivation properties of Al_2O_3 [25–30], more detailed studies that analyze the different physical effects involved are needed. Although in the literature there are several studies showing that bulk recombination is the limiting effect in the electrical performance of CIGS solar cells [31–34] and that the interfaces are not problematic [35], recent experimental reports show that improved CIGS interface passivation can actually lead to substantial gains [36,37]. These findings have motivated device simulations that have predicted gains up to 3% (in absolute power conversion efficiency) in fully passivated solar cells [38–41].

Ultrathin devices have recently been studied in detail by numerous groups [42–47] as they have the potential to reduce the material costs and manufacturing times [48]. Ultrathin devices are believed to be the forward path in this CIGS technology as they enable a combination of significant advantages: i) lower material consumption, which is of crucial industrial importance mainly due to In scarcity; ii) increased mechanical flexibility and integration in a broad range of consumer-oriented applications (e.g. BIPV, portable electronics, wearables, internet of things, etc.); iii) increased electrical performance, when the interfaces are fully passivated, due to lower bulk recombination as a consequence of reduced CIGS thickness. Besides, ultrathin CIGS devices are the ideal test bed to study the effects of rear passivation developments [20], as those investigated here, since their thickness is on the same order of magnitude, or even smaller, than the minority carrier diffusion length, causing carriers to be more exposed to the highly recombinative rear interface. As such, this approach leaves room to study the rear passivation effect in more detail and opens the door to ultrathin devices with enhanced electrical performance.

In this work, we study in depth the effects of the CIGS solar cells rear interface passivation based on a nanopatterned point contact Al_2O_3 layer. Most notably we correlate the effects of the solar cells with an optical model and photoluminescence measurements which allowed us to infer a number of properties of the interface passivation effects on the electrical performance of ultrathin solar cells.

Results

Two types of solar cells were prepared: a) a reference solar cell with the standard CIGS solar cell structure; b) a solar cell with an Al_2O_3 nanopatterned layer in-between the Mo and the CIGS, the so-called passivation layer, as represented in Fig. 1. The Al_2O_3 layer was nanopatterned using e-beam lithography and a dry etching process to produce openings of ~400 nm with a pitch of 2000 nm. The ultrathin CIGS absorber layer is 350 nm thick, so that the effects of rear interface recombination have a stronger impact on the cell performance. Moreover, the CIGS layer has no elemental gradients. The importance of having flat, ungraded, profiles, is to avoid complementary rear surface passivation effects as those that would be caused by the quasi-electric field of the Ga gradient [49]. We highlight the fact that with the exception of the passivation layer, all the solar cell processing was exactly the same for both solar cells.
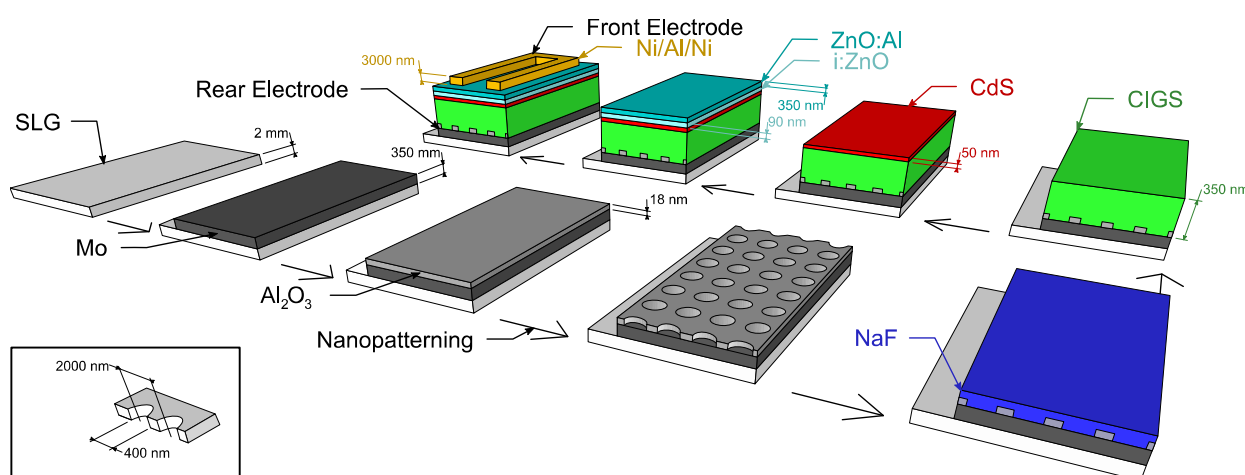

Figure 1: Representation of the solar cell fabrication process of the passivated solar cell. The reference device excluded the Al_2O_3 deposition and the nanopatterning steps.

Fig. 2) shows a cross section high angle annular dark-field (HAADF) TEM image of the passivated solar cell. All of the solar cells layers, Mo, Al_2O_3, CIGS, CdS and the ZnO are visible, together with the TEM preparation layers. We note that a layer consisting of Mo and Se with a thickness value between 15 to 25 nm is visible in the Mo/CIGS interface exposed by the point contacts. The bright layer on the bottom is the rear contact, Mo, and on top the passivation layer with the nanopatterned openings is visible as a dark line. The openings, or point contacts, in the 18 nm thick Al_2O_3 layer have

an equivalent area similar to a circle of 400 nm as defined during the exposure and etching. Since the Al_2O_3 is an insulator, the openings allow for electrical contact between the rear contact and the CIGS absorbing layer. The TEM image showing the presence of the Al_2O_3 layer demonstrates that the Al_2O_3 layer with the nanopatterned contacts is sufficiently robust to withstand the harsh CIGS growth conditions, i.e. 530 °C in a Se atmosphere.
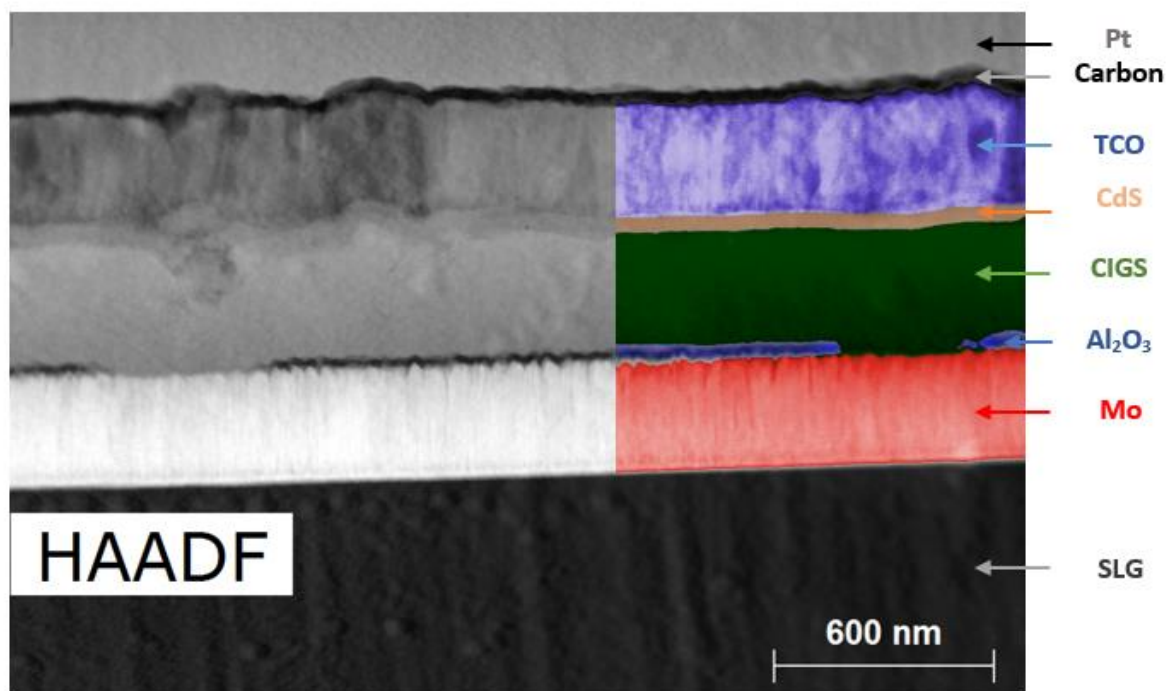

Figure 2: TEM HAADF image of the cross-section of the passivated solar cell. The dark layer in-between the Mo layer and the CIGS layer, is the Al_2O_3 passivation layer. The observed openings on this Al_2O_3 layer are the nanopatterned point contacts.

Solar cell results

Fig. 3a) shows representative J-V curves and Fig. 3b) the corresponding EQE spectra of devices with and without the passivation layer. The inset of Fig. 3a) shows average values together with standard deviations of the figures of merit of the solar cells. The shown curves are representative and were chosen with J-V parameters close to the average values. Both cells show good diode-like behavior without any evidence of blocking behavior. Despite good FF (> 70%) and moderate V_{OC} values

(> 500 mV), we note that the efficiency of both cells is being limited mostly by low J_{SC} values (< 21 mA/cm^2). We attribute the low J_{SC} values due to the very thin CIGS layer, 350 nm, which is not sufficient to fully absorb incoming light, in contrast with that (~2 μm thick) used in conventional CIGS cells. Such relatively thin layer leads to high optical losses in the near infrared region. These absorbers are also heavily affected by rear interface recombination, making them ideal to evaluate the effects of the passivation layer. The differences between the two cells are striking, the reference cells achieve, in average, an efficiency value of 7.5% whereas the passivated devices exhibit a value of 9.7%. This large increase in efficiency is due to an increase from 538 mV to 627 mV in V_{OC}, and an increase from 19.29 mA/cm^2 to 21.56 mA/cm^2 in J_{SC}. The difference in the J_{SC} is seen in the EQE, since the passivated solar cell has a superior performance than the reference cell throughout the most of the spectrum. In terms of standard deviations, both cells have similar variations in terms of V_{OC}, the passivated solar cell has a higher deviation of results in J_{SC} but a smaller one in FF. This translates into a smaller spread of efficiency values for the passivated solar cell showing more uniform results. The J-V analysis shows that the passivation procedure is beneficial and produces devices with a superior electrical performance in terms of V_{oc} and J_{SC}. It can be pointed out that the passivated devices are quite stable, one year after their fabrication and first measurements, the electrical performance was, within error measurements, the same.

C-V measurements were also performed on all solar cells and the CIGS doping concentration was extracted at the 0 V point [50]. The reference device has a median CIGS (apparent) doping concentration at 0 V of 3.2×10^{16} cm^{-3} with a standard deviation of 0.3×10^{16} cm^{-3} whereas the passivated devices present an average of 1.9×10^{16} cm^{-3} with a standard deviation of 0.3×10^{16} cm^{-3}. These values are close to error values of the measurement and show that the Na concentration of the two solar cells is similar.

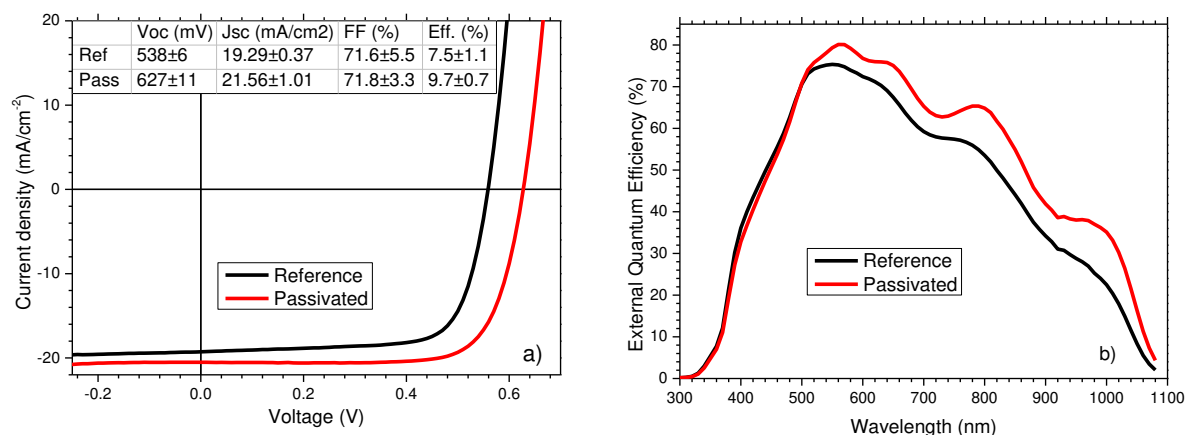|	Voc (mV)	Jsc (mA/cm2)	FF (%)	Eff. (%)
Ref	538±6	19.29±0.37	71.6±5.5	7.5±1.1
Pass	627±11	21.56±1.01	71.8±3.3	9.7±0.7

Figure 3: a) J-V curves of representative cells and the table shows averages with standard variation values of J-V parameters for 12 cells. b) EQE of the same representative devices shown in a).

Optical simulations

In order to further understand the J_{SC} gain of the passivated solar cells, we performed detailed electromagnetic simulations to verify if the attained current gains are due to optical (e.g. from an increased reflection and/or back scattering of the rear contact) or electronic effects caused by the passivation layer. The computations were performed with a FDTD mesh-based solver, as discussed further elsewhere [51,52]. The simulated structure was based in the dimensions of the solar cells: ZnO thickness of 440 nm; CdS 70 nm; CIGS 350 nm; $MoSe_2$ 25 nm or Al_2O_3 18 nm; Mo 350 nm [53], in agreement with the TEM image of Fig. 2). The complex refractive index (n,k) values of CIGS with [Ga]/([Ga]+[In]) = 0.31 were taken from [54].

The simulation results are given in Fig. 4a,b), which shows the photo-carrier generation rate profiles and light absorption spectra along the corresponding solar cells stack, for devices with and without (reference) the passivation layer. Only the light absorbed in the GIGS (termed useful absorption) leads to significant photo-current. The parasitic light absorption by the solar cell stack that does not translate into photo-current occurs mainly in: i) the UV range due to the light absorption in the ZnO-based transparent conductive oxide (TCO) and in the CdS layer, where the low minority carrier lifetime does not allow for current output; ii) the near-infrared (NIR) range due to both the free

8

carriers light absorption in the TCO layer [55,56] and the absorption of the Mo rear contact [57,58]. These optical losses account for the difference shown in Fig. 4b) between the light absorption of the CIGS layer and that in the complete solar cell stack.

One of the initial studies performed with the simulations was the investigation of the contribution of the CIGS material inside the point contact in the overall cell absorption, and its possible optical influence in the rest of the CIGS layer. Even though the openings correspond to a very small area, they could create a sub-wavelength effect that is worth exploring. For that, we simulated Al_2O_3 passivation layers with and without the hole and arrived to the conclusion that, at least optically, the extra CIGS placed inside the Al_2O_3 layer does not significantly influence the absorption spectra. On the simulation of the structures shown in Fig. 4a) and if we consider a unitary internal quantum efficiency (IQE = 1) in the range of 300 to 1100 nm, i.e. all the light absorbed by the CIGS would generate carriers, we would reach an optical J_{SC} value of 28.50 mA/cm^2 for the reference solar cell and 29.40 mA/cm^2 for the passivated solar cell. Such computed J_{SC} values are obviously higher than those measured in Fig. 3a) since they only account for optical effects and neglect electrical losses. The higher simulated J_{SC} value attained by simulating the passivated solar cell structure is due to its improved reflection, by light interference fringes, occurring at NIR wavelengths (700-1000 nm), see Fig. 4b). Such interference fringes are caused by the improvement of the reflection from the rear Al_2O_3/Mo surface. Experimentally, the increased interference fringes in the same wavelength region for the passivated solar cell are visible in Fig. 3b), also demonstrating a good fit of the simulation with the experimental results.
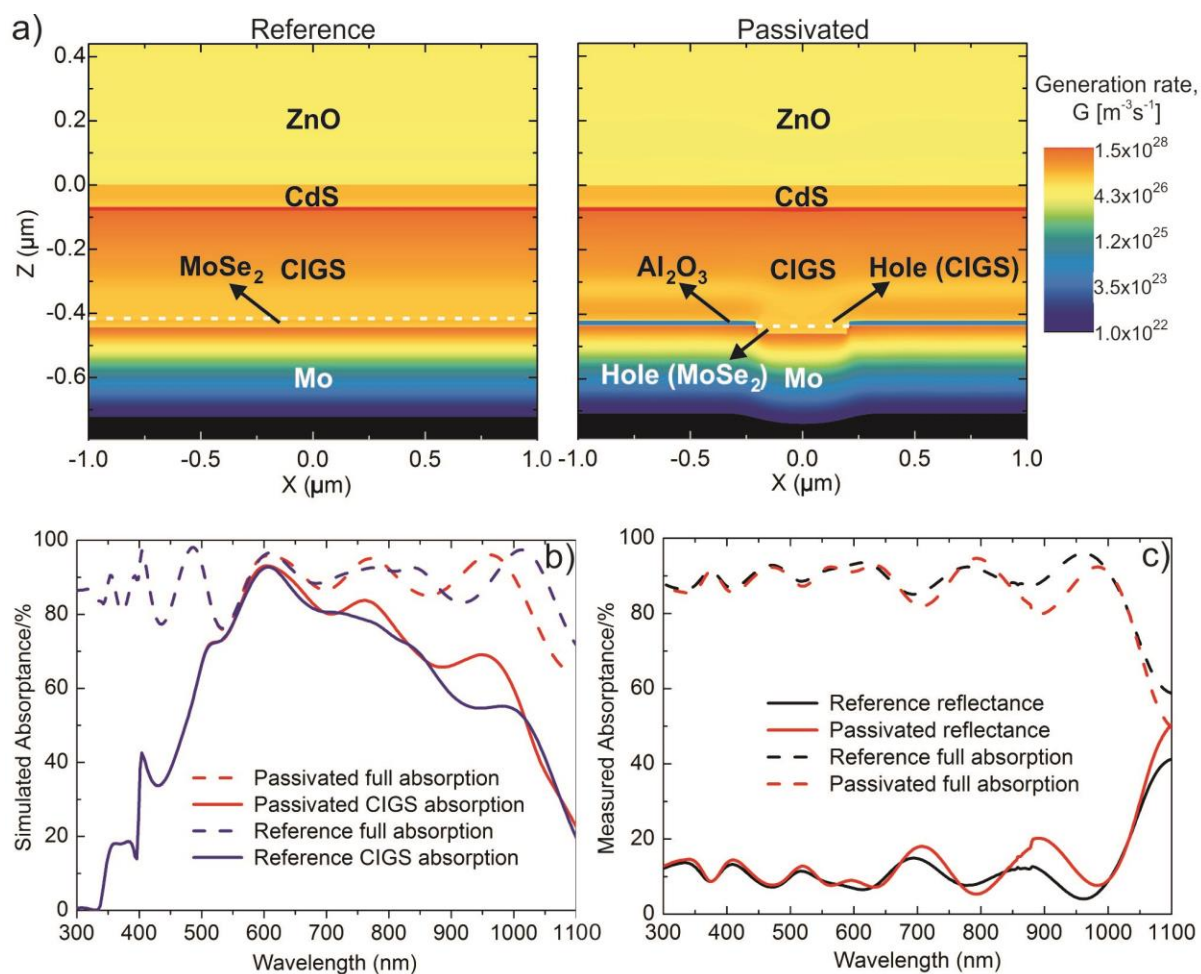
Figure 4: Optical results for the two solar cell structures without (reference cell) and with the passivation layer (passivated cell). a) Computed carrier generation profiles for both analyzed device structures. b) Simulated light absorption of the full solar cell stacks (dashed lines, total absorption) and of only the CIGS layer (solid lines, useful absorption) for the two device structures with and without the passivation layer. c) Corresponding measured/experimental total absorptance (100% - total reflection).

It should be noted that the difference between the simulated J_{SC} values (0.9 mA/cm^2) is significantly lower than that between the measured J_{SC} values (~2.3 mA/cm^2) in Fig. 2a). Therefore, such J_{SC} difference observed in the J-V measurements cannot be ascribed merely to optical effects and should be also caused by the electrical passivation behavior of the Al_2O_3 nanopatterned layer.

Photoluminescence

Photoluminescence probes the electronic structure of semiconductors and can be used to arrive to a qualitative evaluation of the effects of passivation layers, in particular to the influence of defects, being those radiative or non-radiative. The normalized PL spectra of the two solar cells, measured at 7 K, under an excitation power of 29 mW and equivalent experimental conditions, are presented in Fig. 5a). Two broad and asymmetric bands with a maximum intensity at 1.07 and 1.06 eV are observed for the reference and passivated solar cells, respectively. Broad emission is typical of Cu-poor CIGS polycrystalline solar cells [42], [43], however, for the case of the reference solar cell, the luminescence is significantly broader than that of the passivated cell. Additionally, the reference solar cell also shows a larger asymmetry in the low energy side of the spectrum suggesting the existence of a higher influence of defects [62,63]. Regarding the passivated solar cell, the full width at half maximum (FWHM) is significantly lower (~61 meV) than that of the reference solar cell (~96 meV). With the increase of temperature (Fig. 5b)), the FWHM value of both solar cells increases, as expected. Still, at higher temperatures, in the case of the passivated solar cells, the shape of the luminescence band is very similar to the one measured at low temperature, although with a slight redshift, while for the reference solar cell there are significant changes that further indicate the presence of additional radiative transitions. Since the CIGS layer is nominally the same, the changes in PL must be related with the passivation of the rear surface of the absorber layer. In the literature, in addition to the shape of the PL emission at low temperature, to infer the effect of the passivation layer, quite often a comparison of the PL intensity is performed [64–68]. However, a direct comparison of PL intensity from different samples should be done with caution due to the necessarily different optical alignments despite nominally equivalent experimental conditions and as in this work we do not have those capabilities we do not perform that comparison here. With the used excitation wavelength, 514.5 nm, penetration depth of the incident photons, ~70 nm, is smaller than the CIGS thickness, 350 nm. However, the generated charge carriers are influenced by the modification of the density of interface defects induced by the Al_2O_3 deposition due to the CIGS high carrier diffusion length [69,70] suggesting

a different electronic structure in both solar cells caused by the passivation of the rear interface which lowers the interface defects concentration.
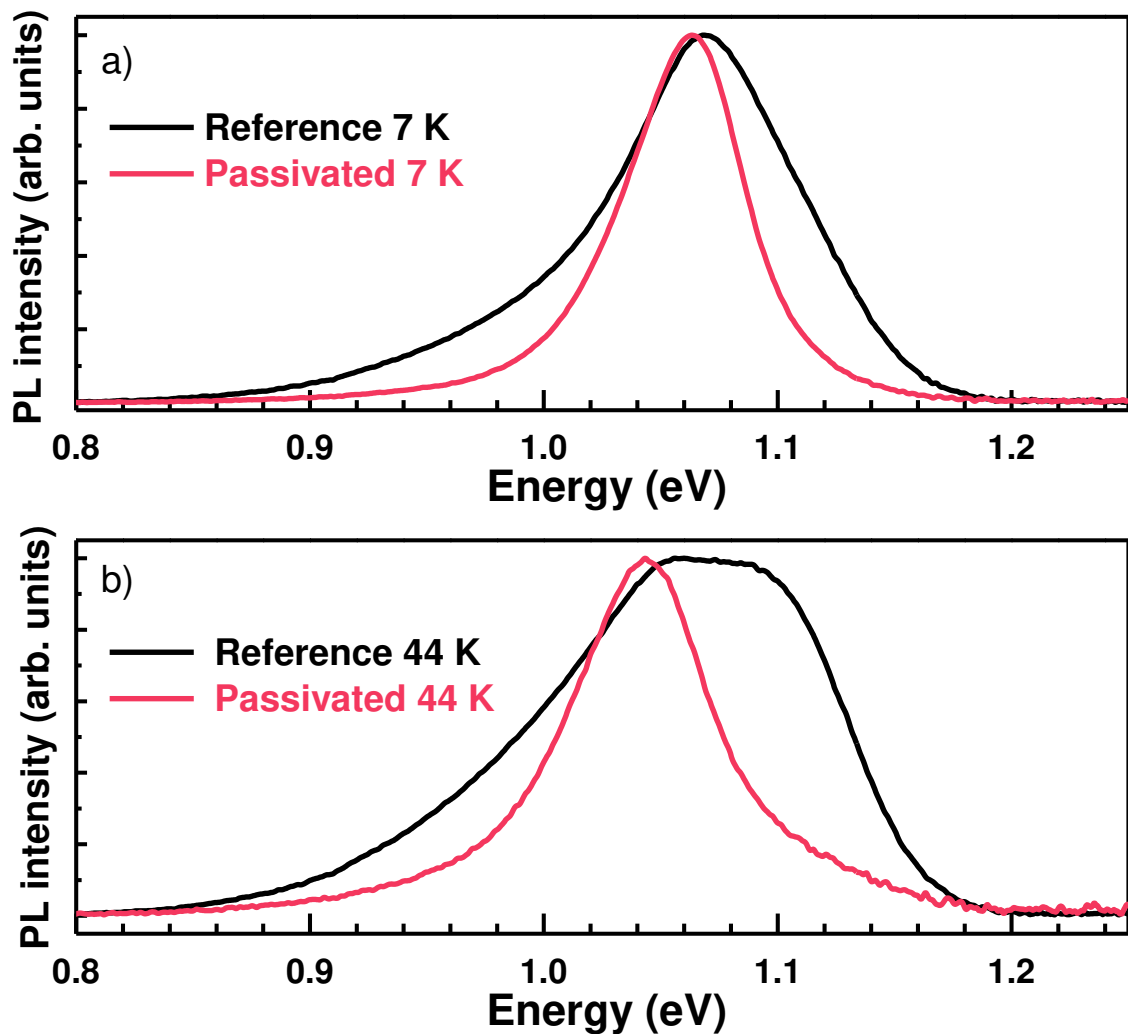

Figure 5: Normalized PL spectra of the reference and passivated solar cells under an excitation power of 29 mW and measured at: a) 7 K; b) 44 K.

Discussion

Since both devices have exactly the same layers except the rear Al_2O_3 passivation layer, we link the differences in the cells performance directly to the effect of the passivation layer. The passivation vastly reduces the total electrical contacting area but, remarkably, the FF values of both cells are still acceptable and very similar, 71.6% for the reference and 71.8% for the passivated one. A good FF value is a sign that the contacting area is well defined. In contrast, low FF values, together

with evidences of series resistance, are good indications of point contact structures which are not optimized[71]. For the passivated solar cell, these high values of FF show that the nanopatterned passivation layer in terms of density and spacing design forms an effective contacting area. However, we note that there is a difference of 89 mV between both devices in V_{OC}. With an increase of V_{OC}, FF is expected to follow. Using the well-known equation that relates V_{OC} with FF [72,73]:

$$FF = \frac{v_{oc} - ln(v_{oc} + 0.72)}{v_{oc} + 1}$$

where v_{oc} is the normalized voltage defined as $V_{oc}/(AkT/q)$, A is the ideality factor of the cell, k the Boltzmann's constant, T the temperature and q the electron charge and considering the ideality values, A, of 0.92 and 1.13 for the reference and the passivated cell, respectively, it is possible to estimate that the passivated device should have a FF value around 3% higher than the passivated solar cell due to its higher V_{OC} value. Hence, more optimization to increase the value of the FF of the passivated devices has to be made by for instance tuning the thickness of the Al_2O_3 layer and the dimensions of the nanopattern, which could improve the non-ideal rear contact resistance, or by tuning of the alkali content. With regards to J-V behavior, we note that the reference cell shows some signs of shunting which are not present in the passivated cell. However, a dark J-V measurement of the reference device showed no evidence of shunting. Such fact is a good indication that instead of shunting, the reference cells are being affected by voltage-dependent current collection (VDCC). VDCC occurs in devices with low values of effective diffusion length and with negligible recombination losses in the space-charge-region. In these conditions, a small change in voltage creates a different depletion region contributing thus to different current collection. Low values of effective diffusion length can be caused either by high bulk- or rear interface-recombination. Thus, we attribute the VDCC of the reference device to its high rear interface recombination. As the rear interface recombination is suppressed in the passivated solar cell, it does not suffer from VDCC.

V_{OC} and J_{SC} values are higher for the solar cells with the passivation layer, well above uncertainty and the standard deviations values. Concerning the V_{OC} values, the 89 mV difference

between both devices can undoubtedly be attributed to effects caused by the introduction of the Al_2O_3 layer. The increase of V_{OC} values in devices after the introduction of a passivation layer is something expected and very well known in other type of solar cells due to lower interface recombination [74,75]. With respect to the J_{SC} difference, the EQE results (Fig. 2b)) shows that the gains of the passivated cells are from wavelength values above 500 nm. Such region is the optical region above the absorption edge of the CdS buffer layer. Having the gains distributed throughout almost all of the spectral range is a confirmation of the simulation results that the increase of the J_{SC} is not only due to enhanced optical rear reflection, but also due to electronic effects. Three improvements could lead to such an increase of J_{SC}: i) a lowering of the rear contact interface defect density allowing for a lower effective interface recombination velocity; ii) an increased effective minority carrier diffusion length due to an effective electric field at the rear contact induced by negative charges in the passivation layer; iii) an increased optical reflection of the rear contact. Increased optical reflection would be of high interest as it is one of the limitations of ultrathin CIGS solar cells [76–82]. In fact, several approaches have been tested in order to increase the reflection and light scattering properties of the rear contact [24,83–88]. Such properties can contribute to the enhancement of the optical path length of mostly the weakly-absorbed near infra-red (NIR) photons within the CIGS region, thus enabling higher EQE in the NIR range close to the CIGS bandgap (> 700 nm), as seen in the optical results of Fig. 4b,c). However, our results of Fig. 3b) show a photocurrent increase even for wavelengths down to 500 nm, a region where no optical losses are expected. The optical simulations agree with the interpretation that the increase in J_{SC} of the passivated cell cannot be solely attributed to an increased reflection, as commented in the optical analysis section. Therefore it can be concluded that the effect of introducing the point contact layer increases device performance by somewhat increasing the rear reflection but also significantly by the effect of its electronic passivation role, in agreement with our previous studies [20,89] and contrary to other data interpretation from the literature [35].

Another scenario that needs to be addressed is the Na diffusion blocking properties of the Al_2O_3 layer. One would expect the passivated solar cell to have a lower Na concentration than the

reference one. To understand this effect, we focus on the apparent doping concentration values extracted by the C-V measurements. Such measurement shows very similar doping concentration which points towards Na concentration values of both solar cells to be also identical. It has been shown that by introducing Na using a NaF precursor layer with a thickness of 15 nm and 22.5 nm would lead to an increase of V_{OC} of 1 mV and an apparent carrier concentration increase around 1×10^{16} cm^{-3} [90]. The experimental difference seen in this work between the reference and the passivated devices is 1.3×10^{16} cm^{-3}, hinting at the fact that the carrier concentration is not changing the V_{OC} values significantly. Even if the previous experimental results cannot be directly linked to the one presented here due to the ultrathin CIGS layers, since the reference device is actually the one with the higher carrier concentration, using the expression:

$$\Delta V_{OC} = \frac{K_B T}{q} ln\left(\frac{N_{ref}}{N_{pass}}\right)$$

where K_B is the Boltzmann's constant, T temperature and q the elemental charge, a V_{OC} difference of 13 mV higher for the reference cell compared with the passivated solar cell can be calculated. Thus, both from previous experimental results and the previous calculation, if the passivated solar cell has a lower amount of Na compared with the reference solar cell, it would be expectable to have a lower V_{OC}. Accordingly, even if there are small differences in the Na content of the two solar cells, its influence on the carrier concentration leads to V_{OC} changes that are contrary to the ones seen by the J-V analysis. From both arguments, we conclude that the V_{OC} differences seen here cannot be explained by differences in Na and/or carrier concentration.

Regarding the PL interaction volume, if we give thought only to optical considerations, the PL analysis would only analyze a top surface layer of 70 nm [91]. However, the fact that the PL measurements are affected by modifications to the rear contact show that the CIGS has a minority carrier diffusion length high enough to allow photo-generated carriers at the surface of the CIGS layer to still interact with the rear contact. This result contrasts with previous observations that the PL could contribute with in-depth probing [92]. However, such procedure was applied to kesterite compounds

with a low electrical performance, which are known to have a lower minority carrier diffusion length and significant lower electrical performance than the one of CIGS [93]. Interestingly, the fact that PL is sensitive to the entire CIGS volume is in good agreement with the EQE results. The EQE shows that for all the incoming wavelengths there is a superior quantum efficiency for the passivated solar cells. Low wavelength values (~500-600 nm), or high energy photons, correspond to light absorption in the CIGS close to the surface, but even there the EQE behavior of the passivated cell is superior. This effect is in full agreement with the PL being also sensitive to changes in the rear interface, as expected in the case where the effects are made in a distance smaller to the carriers diffusion length.

The PL analysis has shown qualitatively that the passivation reduces the number of radiative defects that are active in the CIGS. Such reduction of the number of interface defects by the rear passivation was shown by PL: i) as a larger FWHM value of the reference solar cell, compared with the passivation one, and ii) by the appearance of additional radiative transitions as the temperature increases for the reference solar cell. Concerning the FWHM for the PL in both solar cells, the widening of the PL emission has been directly linked in the literature to worse solar cell performances [94]. We observe that the reference cell has a FWHM of ~96 meV and has an efficiency of 7.5%, whereas the passivation solar cell has an FWHM of ~61 meV and with an efficiency of 9.7%. This relation establishes that the passivation strategy lowers the numbers of active interface defects that rule the CIGS optical-properties leading to a higher solar cell performance. Thus, we can conclude that the Al_2O_3 nanopatterned point contact layer lowers the interface recombination at the CIGS rear interface. This results, is in very good agreement with our previous observation using electrical measurements of a lower trap density for CIGS/Al_2O_3 interfaces [95].

Further work should focus on understanding the properties of the Al_2O_3 passivation layer after it is exposed to the harsh CIGS growth conditions. These growth conditions, a temperature of 525 ^{o}C in a Se atmosphere, have been linked to a change in the electronic properties of the AL_2O_3 layer [95] and in other dielectric materials, it is known that the inclusion of mid-gap defects significantly changes

16

the material properties even by changing it from an electrical insulator to a conductor compound [96,97]. Hence, a full understanding of the electronic properties of the AL_2O_3 layer after being exposed is needed to further expand the understanding of this system.

Conclusions

Ultrathin CIGS based solar cells with and without passivation layers were fabricated. The passivation consisted of a nanopatterned 18 nm Al_2O_3 layer with an array of point contacts that allows for electrical contacting between the CIGS and the Mo layer. By comparing the passivated solar cells with the reference devices, we conclude that the Mo-CIGS state-of-the-art interfaces are highly recombinative and that only with an effective passivation scheme, ultrathin CIGS devices can achieve high values of electrical performance. Such fact was observed here by combining optical simulations with the results of experimental devices. Firstly, the difference in electrical performance of both devices shows that by comparing a passivation device with a non-passivated device, the passivation increases both V_{OC} and J_{SC}. Secondly, the conjugation of the EQE results with the optical simulations shows that the passivation layer improves the NIR light reflection from the rear contact. However, the simulations also show that the improvement in reflection alone is not sufficient to fully justify the total observed increase of the J_{SC} values (2.3 mA/cm^2), which is therefore mainly attributed to electric rather than optical effects. Thirdly, PL measurements show that the passivation reduces the defect concentration allowing for higher V_{OC} values. Another gain with the passivation layer is reduced VDCC, which again is a confirmation of the very low recombinative rear interface of the passivation device. Thus, the combination of the characterization techniques used in this work allowed us to identify that the nanopatterned Al_2O_3 layer is both lowering the concentration of defects and increasing the rear optical reflection.

Altogether, the electrical performance of these cells demonstrates that for ultrathin CIGS the introduction of a rear passivation layer based in a nanopatterned point contact Al_2O_3 layer increases solar cell electrical performance. The introduction of the nanopatterned Al_2O_3 layer passivates the

rear electrical contact allowing for devices with a 350 nm CIGS layer to achieve power conversion efficiency values close to 10%.

Experimental

The solar cells prepared in this work followed the Ångström solar cell baseline, as presented in Fig. 1, and their layer structure was deposited in the same batch [53]. Two sets of solar cells were prepared, one with the regular solar cell structure – designated as reference, and a second one with a passivation layer – designated as passivated solar cell. From each set, 12 solar cells were fabricated. The passivation layer, a 18 nm Al_2O_3 layer, was deposited by atomic layer deposition (ALD) on Mo. The nanopattern was first defined by e-beam lithography and consisted of a square array of openings/holes of ~400 nm diameter separated by 2000 nm among them. Such array allows for ~97% passivated area leaving ~3% of the area for contacting. Afterwards, the structures were open using a dry etching process [98]. The patterned passivation layer is the only difference between both types of solar cells. For the CIGS evaporation, flat evaporation rates were used to avoid having Cu- and Ga-depth profiles [99]. The CIGS composition is [Cu]/([Ga]+[In]) = 0.70 and [Ga]/([Ga]+[In]) = 0.295 as estimated by XRF with a thickness of 350 nm estimated by stylus profilometry. Prior to the CIGS deposition, a 15 nm NaF layer was deposited which served as the Na source for the CIGS doping [100].

Completed solar cell devices were characterized by J–V measurements with AM1.5 illumination in a home-built system. Fill factor (FF), efficiency, short-circuit current density (J_{SC}), and open circuit voltage (V_{OC}) were calculated from the J–V curves and the corresponding values given in Fig. 2a) are the average of 12 cells with their respective standard deviation. External quantum efficiency (EQE) was determined under ambient light, using chopped monochromatic light that was scanned through the wavelength interval of 360–1200 nm in 2-nm steps, also in a home built system. The photoluminescence (PL) measurements were carried out on a Bruker IFS 66v Fourier Transform Infrared (FTIR) spectrometer, equipped with a Ge diode detector. The excitation source was a 514.5 nm line of an Ar^+ ion laser (spot diameter of ~1 mm), with a laser power measured at the front of the

cryostat window. The solar cells were inserted in a helium gas flow cryostat which allowed the change of temperature in the range 7–300 K. The correction of the detectivity of the Ge detector was performed for all spectra. The apparent free carrier density measurements were performed using C-V measurements on an Autolab PGSTAT302N equipped with the FRA32 module. The measurements were performed in dark using a Faraday cage at room temperature. The amplitude of the AC signal was set to be constant and equal to 10 mV rms and the frequency was constant and equal to 10 kHz. The DC component of the excitation signal ranged from -1.0 V to 0.5 V.

Scanning transmission electron microscopy (STEM) images were taken with a FEI Titan Themis 80-300 kV Cs-probe corrected transmission electron microscope (TEM), operating at 200 kV accelerating potential. The lamellae were prepared in a focused ion beam (FIB) FEI Dual-Beam Helios 450S with FIB Mo-grids, using a technique known as "lift-out" [101]. On top of the solar cell, a protective evaporated carbon layer followed by a Pt bi-layer were deposited using the electron beam and the Ga beam [102].

Optical modelling description

A numerical 3D mesh-based finite difference time domain (FDTD) method was employed to model the optical response of the fabricated structures, using a specialized commercial solver [103]. The mesh resolution was adapted to the geometry of the structures and illumination conditions after sets of convergence tests, in order to minimize the computational requirements while maintaining high accuracy. The simulations were corroborated by matching the FDTD optical absorption spectra of the flat multilayered cell structures (without the patterned point contacts) with analytical formalisms based on the transfer matrix method.

The periodicity of the square array of rear point contacts allows the FDTD region to be reduced to a square unit cell with side equal to the array pitch. Specific boundary conditions (BCs) were applied in each face of such region. Artificial absorbing perfect-matching layers were applied on the upper and lower boundaries to absorb all outgoing waves. On the side boundaries, periodic BCs were used to

model the infinite periodicity of the structures. Here, due to the symmetries of the structure at normal incidence, symmetric and anti-symmetric BCs are employed which allow simulating only one quadrant of the unit cell.

Acknowledgements

References

[1]   M. A. Green, Y. Hishikawa, W. Warta, E. D. Dunlop, D. H. Levi, J. Hohl-Ebinger, A. W. H. Ho-Baillie, *Prog. Photovoltaics Res. Appl.* **2017**, *25*, 668.

[2]   R. Kamada, T. Yagioka, S. Adachi, A. Handa, K. F. Tai, T. Kato, H. Sugimoto, in *2016 IEEE 43rd Photovolt. Spec. Conf.*, IEEE, **2016**, pp. 1287–1291.

[3]   P. Reinhard, F. Pianezzi, B. Bissig, A. Chirila, P. Blosch, S. Nishiwaki, S. Buecheler, A. N. Tiwari, *IEEE J. Photovoltaics* **2015**, *5*, 656.

[4]   P. Jackson, R. Wuerz, D. Hariskos, E. Lotter, W. Witte, M. Powalla, *Phys. status solidi - Rapid Res. Lett.* **2016**, *10*, 583.

[5]   J. H. Werner, J. Mattheis, U. Rau, *Thin Solid Films* **2005**, *480–481*, 399.

[6]   M. Gloeckler, J. R. Sites, *Thin Solid Films* **2005**, *480–481*, 241.

[7]   A. Sacco, F. Bella, S. De La Pierre, M. Castellino, S. Bianco, R. Bongiovanni, C. F. Pirri, *ChemPhysChem* **2015**, *16*, 960.

[8]   S. Galliano, F. Bella, C. Gerbaldi, M. Falco, G. Viscardi, M. Grätzel, C. Barolo, *Energy Technol.* **2017**, *5*, 300.

[9]   E. S. Barnard, B. Ursprung, E. Colegrove, H. R. Moutinho, N. J. Borys, B. E. Hardin, C. H. Peters, W. K. Metzger, P. J. Schuck, *Adv. Mater.* **2017**, *29*, 1603801.

[10]   J. M. Burst, J. N. Duenow, D. S. Albin, E. Colegrove, M. O. Reese, J. A. Aguiar, C.-S. Jiang, M. K. Patel, M. M. Al-Jassim, D. Kuciauskas, S. Swain, T. Ablekim, K. G. Lynn, W. K. Metzger, **2016**, *1*, 16015.

[11]   J. Shi, X. Xu, D. Li, Q. Meng, *Small* **2015**, *11*, 2472.

[12]   Y. C. Kim, T.-Y. Yang, N. J. Jeon, J. Im, S. Jang, T. J. Shin, H.-W. Shin, S. Kim, E. Lee, S. Kim, J. H. Noh, S. I. Seok, J. Seo, *Energy Environ. Sci.* **2017**.

[13]   J.-P. Correa-Baena, W. Tress, K. Domanski, E. H. Anaraki, S.-H. Turren-Cruz, B. Roose, P. P. Boix, M. Gratzel, M. Saliba, A. Abate, A. Hagfeldt, *Energy Environ. Sci.* **2017**, *10*, 1207.

[14]   J. Zhang, A. Hultqvist, T. Zhang, L. Jiang, C. Ruan, L. Yang, Y. Cheng, M. Edoff, E. M. J. Johansson, *ChemSusChem* **2017**, DOI 10.1002/cssc.201701160.

[15]   B. Vermang, V. Fjällström, J. Pettersson, P. Salomé, M. Edoff, *Sol. Energy Mater. Sol. Cells* **2013**, *117*, 505.

[16]   P. Casper, R. Hünig, G. Gomard, O. Kiowski, C. Reitz, U. Lemmer, M. Powalla, M. Hetterich, *Phys. Status Solidi - Rapid Res. Lett.* **2016**, *10*, 376.

[17]   B. Vermang, J. T. Wätjen, V. Fjällström, F. Rostvall, M. Edoff, R. Kotipalli, F. Henry, D. Flandre, *Prog. Photovoltaics Res. Appl.* **2014**, *22*, 1023.

[18]   B. Vermang, J. T. Watjen, C. Frisk, V. Fjallstrom, F. Rostvall, M. Edoff, P. Salome, J. Borme, N. Nicoara, S. Sadewasser, *IEEE J. Photovoltaics* **2014**, *4*, 1644.

[19] G. Sozzi, D. Pignoloni, R. Menozzi, F. Pianezzi, P. Reinhard, B. Bissig, S. Buecheler, A. N. Tiwari, *2015 IEEE 42nd Photovolt. Spec. Conf. PVSC 2015* **2015**, 8.

[20] B. Vermang, V. Fjällström, J. Pettersson, P. Salomé, M. Edoff, *Sol. Energy Mater. Sol. Cells* **2013**, *117*, 505.

[21] E. Jarzembowski, B. Fuhrmann, H. Leipner, W. Fränzel, R. Scheer, *Thin Solid Films* **2016**, 2.

[22] J. Kim, S. Park, S. Ryu, J. Oh, B. Shin, *Prog. Photovoltaics Res. Appl.* **2017**, *25*, 308.

[23] G. Yin, M. W. Knight, M.-C. van Lare, M. M. Solà Garcia, A. Polman, M. Schmid, *Adv. Opt. Mater.* **2017**, *5*, 1600637.

[24] G. Yin, M. Song, S. Duan, P. Manley, D. Greiner, C. A. Kaufmann, M. Schmid, *ACS Appl. Mater. Interfaces* **2016**, *8*, 31646.

[25] T.-H. Cheng, W. W. Hsu, C. Y. Huang, J.-A. Lu, J. Y. Chen, C. W. Liu, *ECS Transactions 33* **2011**, pp. 191–197.

[26] A. Hultqvist, T. Sone, S. F. Bent, *IEEE J. Photovoltaics* **2017**, *7*, 322.

[27] J. Keller, F. Gustavsson, L. Stolt, M. Edoff, T. Törndahl, *Sol. Energy Mater. Sol. Cells* **2017**, *159*, 189.

[28] F. Mollica, J. Goffard, M. Jubault, F. Donsanti, S. Collin, A. Cattoni, L. Lombez, N. Naghavi, in *2016 IEEE 43rd Photovolt. Spec. Conf.*, *IEEE*, **2016**, pp. 2213–2217.

[29] W. Ohm, W. Riedel, U. Aksunger, D. Greiner, C. A. Kaufmann, M. C. Lux-Steiner, S. Gledhill, in *2015 IEEE 42nd Photovolt. Spec. Conf.*, *IEEE*, **2015**, pp. 1–5.

[30] W.-W. Hsu, J. Y. Chen, T.-H. Cheng, S. C. Lu, W.-S. Ho, Y.-Y. Chen, Y.-J. Chien, C. W. Liu, *Appl. Phys. Lett.* **2012**, *100*, 23508.

[31] P. M. P. Salomé, V. Fjällström, P. Szaniawski, J. P. Leitão, A. Hultqvist, P. A. Fernandes, J. P. Teixeira, B. P. Falcão, U. Zimmermann, A. F. da Cunha, M. Edoff, *Prog. Photovoltaics Res. Appl.* **2015**, *23*, 470.

[32] M. A. Contreras, K. Ramanathan, J. AbuShama, F. Hasoon, D. L. Young, B. Egaas, R. Noufi, *Prog. Photovoltaics Res. Appl.* **2005**, *13*, 209.

[33] R. Klenk, *Thin Solid Films* **2001**, *387*, 135.

[34] M. Gloeckler, J. R. Sites, *Thin Solid Films* **2005**, *480–481*, 241.

[35]   E. Jarzembowski, B. Fuhrmann, H. Leipner, W. Fränzel, R. Scheer, *Thin Solid Films* **2016**, 2.

[36]   P. Reinhard, F. Pianezzi, B. Bissig, A. Chirila, P. Blosch, S. Nishiwaki, S. Buecheler, A. N. Tiwari, *IEEE J. Photovoltaics* **2015**, *5*, 656.

[37]   B. Vermang, J. T. Watjen, C. Frisk, V. Fjallstrom, F. Rostvall, M. Edoff, P. Salome, J. Borme, N. Nicoara, S. Sadewasser, *IEEE J. Photovoltaics* **2014**, *4*, 1644.

[38]   G. Sozzi, S. Di, R. Menozzi, B. Bissig, S. Buecheler, A. N. Tiwari, *Sol. Energy Mater. Sol. Cells* **2017**, *165*, 94.

[39]   A. Bercegol, B. Chacko, R. Klenk, I. Lauermann, M. C. Lux-Steiner, M. Liero, *J. Appl. Phys.* **2016**, *119*, DOI 10.1063/1.4947267.

[40]   M. Nerat, *Sol. Energy Mater. Sol. Cells* **2012**, *104*, 152.

[41]   T. Umehara, S. Iinuma, A. Yamada, *Electron. Mater. Lett.* **2016**, *12*, 479.

[42]   Z. J. Li-Kao, N. Naghavi, F. Erfurth, J. F. Guillemoles, I. Gérard, A. Etcheberry, J. L. Pelouard, S. Collin, G. Voorwinden, D. Lincot, *Prog. Photovoltaics Res. Appl.* **2012**, *20*, 582.

[43]   J. Posada, M. Jubault, N. Naghavi, *Thin Solid Films* **2017**, *633*, 66.

[44]   N. Naghavi, F. Mollica, J. Goffard, J. Posada, A. Duchatelet, M. Jubault, F. Donsanti, A. Cattoni, S. Collin, P. P. Grand, J. J. Greffet, D. Lincot, *Thin Solid Films* **2017**, *633*, 55.

[45]   E. Jarzembowski, B. Fuhrmann, H. Leipner, W. Fränzel, R. Scheer, *Thin Solid Films* **2017**, *633*, 61.

[46]   O. Lundberg, M. Bodegård, J. Malmström, L. Stolt, *Prog. Photovoltaics Res. Appl.* **2003**, *11*, 77.

[47]   F. Mollica, M. Jubault, F. Donsanti, A. Loubat, M. Bouttemy, A. Etcheberry, N. Naghavi, *Thin Solid Films* **2017**, *633*, 202.

[48]   M. Edoff, S. Schleussner, E. Wallin, O. Lundberg, *Thin Solid Films* **2011**, *519*, 7530.

[49]   O. Lundberg, M. Edoff, L. Stolt, *Thin Solid Films* **2005**, *480–481*, 520.

[50]   P. M. P. Salomé, V. Fjallstrom, A. Hultqvist, P. Szaniawski, U. Zimmermann, M. Edoff, *Prog. Photovoltaics Res. Appl.* **2014**, *22*, 83.

[51]   M. J. Mendes, A. Araújo, A. Vicente, H. Águas, I. Ferreira, E. Fortunato, R. Martins, *Nano Energy* **2016**, *26*, 286.

[52] A. T. Vicente, P. J. Wojcik, M. J. Mendes, H. Águas, E. Fortunato, R. Martins, *Sol. Energy* **2017**, *144*, 232.

[53] J. Lindahl, U. Zimmermann, P. Szaniawski, T. Torndahl, A. Hultqvist, P. Salomé, C. Platzer-Björkman, M. Edoff, *IEEE J. Photovoltaics* **2013**, *3*, 1100.

[54] P. D. Paulson, R. W. Birkmire, W. N. Shafarman, *J. Appl. Phys.* **2003**, *94*, 879.

[55] A. Lyubchyk, A. Vicente, P. U. Alves, B. Catela, B. Soule, T. Mateus, M. J. Mendes, H. Águas, E. Fortunato, R. Martins, *Phys. status solidi* **2016**, *213*, 2317.

[56] A. Lyubchyk, A. Vicente, B. Soule, P. U. Alves, T. Mateus, M. J. Mendes, H. Águas, E. Fortunato, R. Martins, *Adv. Electron. Mater.* **2016**, *2*, DOI 10.1002/aelm.201500287.

[57] K. Orgassa, H. W. Schock, J. H. Werner, *Thin Solid Films* **2003**, *431–432*, 387.

[58] Z. J. Li-Kao, N. Naghavi, F. Erfurth, J. F. Guillemoles, I. Gérard, A. Etcheberry, J. L. Pelouard, S. Collin, G. Voorwinden, D. Lincot, *Prog. Photovoltaics Res. Appl.* **2012**, *20*, 582.

[59] H. Limborço, P. M. P. Salomé, J. P. Teixeira, D. G. Stroppa, R.-R. Andrade, N. Nicoara, K. Abderrafi, J. P. Leitão, J. C. Gonzalez, S. Sadewasser, *CrystEngComm* **2016**, *18*, 7147.

[60] I. Dirnstorfer, M. Wagner, D. M. Hofmann, M. D. Lampert, F. Karg, B. K. Meyer, *Phys. status solidi* **1998**, *168*, 163.

[61] P. M. P. Salomé, V. Fjällström, P. Szaniawski, J. P. Leitão, A. Hultqvist, P. A. Fernandes, J. P. Teixeira, B. P. Falcão, U. Zimmermann, A. F. da Cunha, M. Edoff, *Prog. Photovoltaics Res. Appl.* **2015**, *23*, 470.

[62] J. P. Teixeira, R. A. Sousa, M. G. Sousa, A. F. da Cunha, P. A. Fernandes, P. M. P. Salomé, J. P. Leitão, *Phys. Rev. B* **2014**, *90*, 235202.

[63] J. P. Teixeira, R. A. Sousa, M. G. Sousa, A. F. da Cunha, P. A. Fernandes, P. M. P. Salomé, J. C. González, J. P. Leitão, *Appl. Phys. Lett.* **2014**, *105*, 163901.

[64] J. Joel, B. Vermang, J. Larsen, O. Donzel-Gargand, M. Edoff, *Phys. Status Solidi - Rapid Res. Lett.* **2015**, *9*, 288.

[65] S. Luo, C. Eisler, T.-H. Wong, H. Xiao, C.-E. Lin, T.-T. Wu, C.-H. Shen, J.-M. Shieh, C.-C. Tsai, C.-W. Liu, H. A. Atwater, W. A. Goddard, J.-H. Lee, J. R. Greer, *Acta Mater.* **2016**, *106*, 171.

[66]   Y. S. Lee, T. Gershon, T. K. Todorov, W. Wang, M. T. Winkler, M. Hopstaken, O. Gunawan, J. Kim, *Adv. Energy Mater.* **2016**, *6*, 1.

[67]   W.-W. Hsu, J. Y. Chen, T.-H. Cheng, S. C. Lu, W.-S. Ho, Y.-Y. Chen, Y.-J. Chien, C. W. Liu, *Appl. Phys. Lett.* **2012**, *100*, 23508.

[68]   J. Kim, S. Park, S. Ryu, J. Oh, B. Shin, *Prog. Photovoltaics Res. Appl.* **2017**, *25*, 308.

[69]   T. Dullweber, O. Lundberg, J. Malmström, M. Bodegård, L. Stolt, U. Rau, H. W. Schock, J. H. Werner, *Thin Solid Films* **2001**, *387*, 11.

[70]   G. Brown, V. Faifer, A. Pudov, S. Anikeev, E. Bykov, M. Contreras, J. Wu, *Appl. Phys. Lett.* **2010**, *96*, 22104.

[71]   G. Sozzi, S. Di, R. Menozzi, B. Bissig, S. Buecheler, A. N. Tiwari, *Sol. Energy Mater. Sol. Cells* **2017**, *165*, 94.

[72]   M. A. Green, *Solar Cells: Operating Principles, Technology, and System Applications*, Englewood Cliffs, NJ, USA: Prentice-Hall, **1982**.

[73]   P. M. P. Salome, A. Hultqvist, V. Fjallstrom, M. Edoff, B. G. Aitken, K. Zhang, K. Fuller, C. Kosik Williams, *IEEE J. Photovoltaics* **2014**, *4*, 1659.

[74]   S. W. Glunz, D. Biro, S. Rein, W. Warta, *J. Appl. Phys.* **1999**, *86*, 683.

[75]   M. Taguchi, A. Terakawa, E. Maruyama, M. Tanaka, *Prog. Photovoltaics Res. Appl.* **2005**, *13*, 481.

[76]   C. van Lare, G. Yin, A. Polman, M. Schmid, *ACS Nano* **2015**, *9*, 9603.

[77]   G. Yin, P. Manley, M. Schmid, *Sol. Energy Mater. Sol. Cells* **2016**, *153*, 124.

[78]   G. Yin, M. Song, S. Duan, P. Manley, D. Greiner, C. A. Kaufmann, M. Schmid, *ACS Appl. Mater. Interfaces* **2016**, *8*, 31646.

[79]   M. Schmid, *Semicond. Sci. Technol.* **2017**, *32*, 43003.

[80]   N. Barange, V. Ben Chu, M. Nam, I.-H. Ahn, Y. D. Kim, I. K. Han, B. K. Min, D.-H. Ko, *Adv. Energy Mater.* **2016**, *6*, 1601114.

[81]   S. R. Thomas, C.-W. Chen, M. Date, Y.-C. Wang, H.-W. Tsai, Z. M. Wang, Y.-L. Chueh, *RSC Adv.* **2016**, *6*, 60643.

[82]   Y.-C. Wang, H.-Y. Cheng, Y.-T. Yen, T.-T. Wu, C.-H. Hsu, H.-W. Tsai, C.-H. Shen, J.-M.

Shieh, Y.-L. Chueh, *ACS Nano* **2015**, *9*, 3907.

[83]   S. Schleussner, T. Kubart, T. Törndahl, M. Edoff, *Thin Solid Films* **2009**, *517*, 5548.

[84]   B. Vermang, J. T. Wätjen, V. Fjällström, F. Rostvall, M. Edoff, R. Gunnarsson, I. Pilch, U. Helmersson, R. Kotipalli, F. Henry, D. Flandre, *Thin Solid Films* **2015**, *582*, 300.

[85]   C. van Lare, G. Yin, A. Polman, M. Schmid, *ACS Nano* **2015**, *9*, 9603.

[86]   G. Yin, P. Manley, M. Schmid, *Sol. Energy Mater. Sol. Cells* **2016**, *153*, 124.

[87]   M. Schmid, *Semicond. Sci. Technol.* **2017**, *32*, 43003.

[88]   K. Orgassa, H. W. Schock, J. H. Werner, *Thin Solid Films* **2003**, *431–432*, 387.

[89]   C. Frisk, C. Platzer-Björkman, J. Olsson, P. Szaniawski, J. T. Wätjen, V. Fjällström, P. Salomé, M. Edoff, *J. Phys. D. Appl. Phys.* **2014**, *47*, 485104.

[90]   P. M. P. Salomé, A. Hultqvist, V. Fjällström, M. Edoff, B. Aitken, K. Vaidyanathan, K. Zhang, K. Fuller, C. Kosik Williams, *IEEE J. Photovoltaics* **2013**, *3*, 852.

[91]   P. M. P. Salome, J. P. Teixeira, J. Keller, T. Torndahl, S. Sadewasser, J. P. Leitao, *IEEE J. Photovoltaics* **2017**, *7*, 670.

[92]   P. M. P. Salomé, P. A. Fernandes, J. P. Leitão, M. G. Sousa, J. P. Teixeira, A. F. da Cunha, *J. Mater. Sci.* **2014**, *49*, 7425.

[93]   T. Gokmen, O. Gunawan, T. K. Todorov, D. B. Mitzi, *Appl. Phys. Lett.* **2013**, *103*, DOI 10.1063/1.4820250.

[94]   T. Gokmen, O. Gunawan, T. K. Todorov, D. B. Mitzi, *Appl. Phys. Lett.* **2013**, *103*, DOI 10.1063/1.4820250.

[95]   R. Kotipalli, B. Vermang, J. Joel, R. Rajkumar, M. Edoff, D. Flandre, *AIP Adv.* **2015**, *5*.

[96]   Z. Q. Liu, D. P. Leusink, W. M. Lü, X. Wang, X. P. Yang, K. Gopinadhan, Y. T. Lin, A. Annadi, Y. L. Zhao, A. R. Barman, S. Dhar, Y. P. Feng, H. B. Su, G. Xiong, T. Venkatesan, Ariando, *Phys. Rev. B* **2011**, *84*, 165106.

[97]   Z. Q. Liu, W. Lu, S. W. Zeng, J. W. Deng, Z. Huang, C. J. Li, M. Motapothula, W. M. Lü, L. Sun, K. Han, J. Q. Zhong, P. Yang, N. N. Bao, W. Chen, J. S. Chen, Y. P. Feng, J. M. D. Coey, T. Venkatesan, Ariando, *Adv. Mater. Interfaces* **2014**, *1*, DOI 10.1002/admi.201400155.

[98]   B. Vermang, J. T. Watjen, C. Frisk, V. Fjallstrom, F. Rostvall, M. Edoff, P. Salome, J. Borme,

N. Nicoara, S. Sadewasser, *IEEE J. Photovoltaics* **2014**, *4*, 1644.

[99]   P. M. P. Salomé, A. Hultqvist, V. Fjällström, B. Vermang, M. Edoff, B. Aitken, K. Zhang, K. Fuller, C. Kosik Williams, *Sol. Energy Mater. Sol. Cells* **2014**, *123*, 166.

[100] P. M. P. Salome, A. Hultqvist, V. Fjallstrom, M. Edoff, B. G. Aitken, K. Zhang, K. Fuller, C. Kosik Williams, *IEEE J. Photovoltaics* **2014**, *4*, 1659.

[101] S. Bals, W. Tirry, R. Geurts, Z. Yang, D. Schryvers, *Microsc. Microanal.* **2007**, *13*, 80.

[102] P. M. P. Salome, R. Ribeiro-Andrade, J. P. Teixeira, J. Keller, T. Torndahl, N. Nicoara, M. Edoff, J. C. Gonzalez, J. P. Leitao, S. Sadewasser, *IEEE J. Photovoltaics* **2017**, *7*, 858.

[103] "Lumerical Solutions, Inc.," can be found under http://www.lumerical.com/tcad-products/fdtd/.

List of Figures:

Figure 1: Representation of the solar cell fabrication process of the passivated solar cell. The reference device excluded the Al_2O_3 deposition and the nanopatterning steps.

Figure 2: TEM HAADF image of the cross-section of the passivated solar cell. The dark layer in-between the Mo layer and the CIGS layer, is the Al_2O_3 passivation layer. The observed openings on this Al_2O_3 layer are the nanopatterned point contacts.

Figure 3: a) J-V curves of representative cells and the table shows averages with standard variation values of J-V parameters for 12 cells. b) EQE of the same representative devices shown in a).

Figure 4: Optical results for the two solar cell structures without (reference cell) and with the passivation layer (passivated cell). a) Computed carrier generation profiles for both analyzed device structures. b) Simulated light absorption of the full solar cell stacks (dashed lines, total absorption) and of only the CIGS layer (solid lines, useful absorption) for the two device structures with and without the passivation layer. c) Corresponding measured/experimental total absorptance (100% - Total Reflection).

Figure 5: Normalized PL spectra of the reference and passivated solar cells under an excitation power of 29 mW and measured at: a) 7 K; b) 44 K.